A Radially-Dependent Dispersive Finite-Difference Time-Domain Method for the Evaluation of Electromagnetic Cloaks

Christos Argyropoulos, *Student Member, IEEE*, Yan Zhao, *Member, IEEE*, and Yang Hao, *Senior Member, IEEE*

***Abstract*—A radially-dependent dispersive finite-difference time-domain (FDTD) method is proposed to simulate electromagnetic cloaking devices. The Drude dispersion model is applied to model the electromagnetic characteristics of the cloaking medium. Both lossless and lossy cloaking materials are examined and their operating bandwidth investigated. It is demonstrated that the perfect "invisibility" of electromagnetic cloaks is only available for lossless metamaterials and within an extremely narrow frequency band.**

***Index Terms*—Cloaking, finite-difference time-domain (FDTD), metamaterials.**

I. Introduction

OVER the last two years, cloaking devices have received unprecedented attention from the scientific community. Linear coordinate transformations have been applied, in order to manipulate the electromagnetic characteristics of the propagation medium [1]–[3]. These techniques originate in the theory of General Relativity and conformal mapping procedures. After the transformations, the medium produced (that is, the cloaking shell), is able to guide the electromagnetic waves around an object without any disturbances and reflections. This is equivalent to waves propagating through free space. Hence, the object placed inside the cloak becomes practically "invisible" to an exterior viewer. The permittivity and permeability of such a cloaking device are anisotropic and dispersive, as first demonstrated by Pendry *et al.* [1].

The most appropriate materials for the production of the cloak's exotic electromagnetic characteristics are metamaterials [4]. They are artificially constructed materials with extraordinary electromagnetic properties that cannot be obtained in nature. In practice, it is easier to implement the cloaking device when some (or most) of the parameters are independent of radius. To solve this problem, reduced parameter sets were proposed in [5]–[7], operating with different polarizations. A simplified cloaking device was constructed and tested at microwave frequencies, with promising results [8]. Currently, there are efforts for an experimental verification of cloaking at optical frequencies. One method uses silver nanowires with subwavelength dimensions embedded in a silica dielectric host [6]. Another approach uses a concentric structure made of a layered gold-dielectric material [9]. Recently, cloaks derived from a higher-order coordinate transformation [10] have been proposed for a future optical cloaking device [11]. Indeed, it seems that the scientific community is one step closer to the impossible achievement of "invisibility," which before could only have been part of a science fiction scenario.

However, metamaterials are dispersive, which directly leads to limited bandwidth. These limitations are thoroughly analyzed in [12] and [13]. Another drawback of metamaterials is their lossy nature. Furthermore, the ideal cloaking realization is impossible in theory, due to the wave nature of light [14]. To avoid using metamaterials, an alternative approach was proposed [15], constructing the cloaking shell from layers of homogeneous isotropic materials with subwavelength dimensions. However, it is difficult to realize this structure, due to the alternating different values of permittivity required for the layers of the cloaking device. A different approach, which applied sensors and active sources near the surface of the cloaked object, has been described in [16] and can be functional in a broader bandwidth. Finally, wider bandwidth cloaking applications can be achieved, if the hard surface (metasurface) concept [17]–[19] is employed to construct the cloaking device.

The proposed coordinate transformation technique [1], [2] was also used for the construction of elliptic [20] and square [21] cloaks. Moreover, it has been applied to achieve cloaking in the acoustic frequency spectrum [22], [23]. Based on the coordinate transformation technique, numerous novel applications have been proposed in the literature. The design of magnifying perfect and super lenses has been presented in [24] and [25]. A "rotation coating," derived with the same method of the implemented cloaking shell, has been described in [26]. A concentrator matched with free space has been discussed in [21] and the design of conformal antennas in [27]. Furthermore, a reflectionless complex medium, which can be utilized as an optical beam shifter or a beam splitter, has been introduced in [28].

Until now, the lossless cloaking structure has been modeled analytically [1], [2] and [29]. A cylindrical wave expansion technique was used to simulate a lossless cylindrical cloak in [30]. An analytical method, based on the Mie scattering model, was proposed to exploit the lossy spherical [31] and cylindrical [32] cloaking structures. The commercial simulation package COMSOL Multiphysics has been widely used to

Manuscript received May 12, 2008; revised December 02, 2008. Current version published May 06, 2009.

The authors are with the Antenna Engineering Group, Department of Electronic Engineering, Queen Mary, University of London, London E1 4NS, U.K. (e-mail: y.hao@elec.qmul.ac.uk; Website: http://www.elec.qmul.ac.uk).

Color versions of one or more of the figures in this paper are available online at http://ieeexplore.ieee.org.

Digital Object Identifier 10.1109/TAP.2009.2016704

model different cloaks and to compare theoretical predictions [5], [6], [10], [20] and [21]. It uses the finite element method (FEM), a frequency-domain numerical method. However, such frequency domain techniques can become inefficient if a wide-band solution is desirable. The cloak has also been modeled analytically in the time-domain [33], using a time-dependent scattering theory. The cloaking structure was first simulated with the finite-difference time-domain (FDTD) method in [34]. Another FDTD cloaking model, employing the Lorentz dispersive model, is presented in [35]. In this paper, we propose a new radially-dependent dispersive FDTD method to model lossless and lossy cloaking devices and evaluate their bandwidth limitations. The auxiliary differential equation (ADE) method [36] is used, based on the Drude model, to produce the updating FDTD equations. This dispersive FDTD method is a more general approach to the previously proposed numerical technique [34] and improves on it. The proposed method is able to fully exploit the cloaking phenomenon.

II. Numerical Modeling of the Lossy Cloaking Structure

The FDTD method is based on the temporal and spatial discretization of Faraday's and Ampere's Laws, which are

$$\nabla \times \bar{E} = -\frac{\partial \bar{B}}{\partial t} \tag{1}$$

$$\nabla \times \bar{H} = \frac{\partial \bar{D}}{\partial t} \tag{2}$$

where $\bar{E}$, $\bar{H}$, $\bar{D}$ and $\bar{B}$ are the electric field, magnetic field, electric flux density and magnetic flux density components, respectively. Note that harmonic time dependence $\exp(\jmath\omega t)$ of the field components is assumed throughout this paper. For the dispersive FDTD method, the constitutive equations have also to be discretized; they are given by the following equations:

$$\bar{D} = \varepsilon \bar{E} \tag{3}$$

$$\bar{B} = \mu \bar{H} \tag{4}$$

where the permittivity ε and permeability μ can have scalar or tensor form. For the following cloaking structure modeling, the ADE FDTD technique was employed. Faraday's and Ampere's Laws were discretized with the common procedure [37]; the conventional updating FDTD equations are

$$H^{n+1} = H^n - \left(\frac{\Delta t}{\mu}\right) \cdot \widetilde{\nabla} \times E^{n+\frac{1}{2}} \tag{5}$$

$$E^{n+1} = E^n + \left(\frac{\Delta t}{\varepsilon}\right) \cdot \widetilde{\nabla} \times H^{n+\frac{1}{2}} \tag{6}$$

where Δt is the temporal discretization, $\widetilde{\nabla}$ is the discrete curl operator and n the number of the current time step.

The full set of electromagnetic parameters of the cloaking structure, in cylindrical coordinates, is given by the following [5]:

$$\varepsilon_r(r) = \mu_r(r) = \frac{r - R_1}{r}, \quad \varepsilon_\phi(r) = \mu_\phi(r) = \frac{r}{r - R_1}$$

$$\varepsilon_z(r) = \mu_z(r) = \left(\frac{R_2}{R_2 - R_1}\right)^2 \frac{r - R_1}{r} \tag{7}$$

where R_1 is the inner radius, R_2 the outer radius and r an arbitrary radius of the cloaking structure. The ranges of the cloaking parameters were derived from (7)

$$\varepsilon_r, \mu_r \in \left[0, \frac{(R_2 - R_1)}{R_2}\right], \quad \varepsilon_\phi, \mu_\phi \in \left[\frac{R_2}{(R_2 - R_1)}, \infty\right]$$

$$\varepsilon_z, \mu_z \in \left[0, \frac{R_2}{(R_2 - R_1)}\right].$$

It is observed that the values of ε_r and μ_r are always less than one as r varies between R_1 and R_2, the values of ε_z and μ_z are less than one for some points of r and the values of ε_ϕ and μ_ϕ are always greater than one, as with conventional dielectrics. Thus, the conventional FDTD method cannot correctly simulate materials with the properties of ε_r, μ_r, ε_z, μ_z and new dispersive FDTD techniques must be employed, as with FDTD simulation of left-handed metamaterials (LHMs) [38]. The parameters were mapped with the well-known and widely-used Drude dispersive material model

$$\varepsilon_r = 1 - \frac{\omega_p^2}{\omega^2 - \jmath\omega\gamma} \tag{8}$$

where ω_p is the plasma frequency and γ is the collision frequency, which characterizes the losses of the dispersive material. The plasma frequency ω_p was varied in order to simulate the material properties of the radially-dependent parameters, as given in (7). The required lossy permittivity can also be presented in an alternative way by the formula $\hat{\varepsilon}_r = \varepsilon_r(1 - \jmath \tan\delta)$, where ε_r is radially-dependent and $\tan\delta$ is the loss tangent of the cloaking material. Substituting this formula into (8) and simplifying gave the following analytical equations for the plasma and collision frequencies:

$$\omega_p^2 = (1 - \varepsilon_r)\omega^2 + \varepsilon_r \omega\gamma \tan\delta \tag{9}$$

$$\gamma = \frac{\varepsilon_r \omega \tan\delta}{(1 - \varepsilon_r)}. \tag{10}$$

From (9) and (10), it is obvious that both plasma and collision frequencies vary according to the radius of the cloaking device. Moreover, the plasma frequency is also dependent on the losses of the material represented by $\tan\delta$ and γ.

The ε_ϕ parameter always has values greater than one and was simulated with the conventional lossy dielectric material model

$$\hat{\varepsilon}_\phi = \varepsilon_\phi + \frac{\sigma}{\jmath\omega} \tag{11}$$

where the parameter ε_ϕ is dependent on the radius of the cloaking shell as in (7) and σ is a measurement of the conductivity losses. The loss tangent for the lossy dielectric material is given by $\tan\delta = \sigma/\omega\varepsilon_\phi$. It is also radially-dependent, because it is a function of the ε_ϕ parameter. The two-dimensional (2-D) transverse electric (TE) polarized incidence was used during simulations, without loss of generality, reducing the non-zero fields to three components E_x, E_y and H_z. For TE wave polarization, only three parameters from the full set (7) are employed: ε_r, ε_ϕ, and μ_z.

The classical Cartesian FDTD mesh was used in the modeling and the previously mentioned parameters were transformed

from cylindrical coordinates (r,ϕ,z) to Cartesian ones (x,y,z), as given below

$$\begin{aligned}\varepsilon_{xx} &= \varepsilon_r \cos^2\phi + \hat{\varepsilon}_\phi \sin^2\phi \\ \varepsilon_{xy} &= \varepsilon_{yx} = (\varepsilon_r - \hat{\varepsilon}_\phi)\sin\phi\cos\phi \\ \varepsilon_{yy} &= \varepsilon_r \sin^2\phi + \hat{\varepsilon}_\phi \cos^2\phi. \end{aligned} \tag{12}$$

Hence, the constitutive equation (3) is given in tensor form by

$$\begin{pmatrix} D_x \\ D_y \end{pmatrix} = \varepsilon_0 \begin{pmatrix} \varepsilon_{xx} & \varepsilon_{xy} \\ \varepsilon_{yx} & \varepsilon_{yy} \end{pmatrix} \begin{pmatrix} E_x \\ E_y \end{pmatrix}. \tag{13}$$

From (13), it can be detected that

$$\begin{cases} \varepsilon_0\varepsilon_{xx}E_x + \varepsilon_0\varepsilon_{xy}E_y = D_x \\ \varepsilon_0\varepsilon_{yx}E_x + \varepsilon_0\varepsilon_{yy}E_y = D_y \end{cases} \tag{14}$$

where $\varepsilon_{xx}, \varepsilon_{xy}, \varepsilon_{yx}, \varepsilon_{yy}$ are given in (12). Substituting ε_r from the Drude model [see (8)] and the lossy dielectric $\hat{\varepsilon}_\phi$ with (11) in the first equation of (14), the following was obtained:

$$\begin{aligned} &\varepsilon_0 \left[\jmath\omega\left(\omega^2 - \jmath\omega\gamma - \omega_p^2\right)\cos^2\phi \right. \\ &\quad \left. + (\jmath\omega\varepsilon_\phi + \sigma)(\omega^2 - \jmath\omega\gamma)\sin^2\phi\right] E_x \\ &\quad + \varepsilon_0 \left[\jmath\omega\left(\omega^2 - \jmath\omega\gamma - \omega_p^2\right) - (\jmath\omega\varepsilon_\phi + \sigma)(\omega^2 - \jmath\omega\gamma)\right] \\ &\quad \times \sin\phi\cos\phi E_y \\ &= \jmath\omega(\omega^2 - \jmath\omega\gamma)D_x. \end{aligned} \tag{15}$$

Next, (15) was divided by the factor $\jmath\omega$ to achieve a simpler lower order FDTD algorithm

$$\begin{aligned} &\varepsilon_0 \left[\left(\omega^2 - \jmath\omega\gamma - \omega_p^2\right)\cos^2\phi \right. \\ &\quad \left. + \left(\varepsilon_\phi\omega^2 - \jmath\omega(\sigma + \varepsilon_\phi\gamma) - \sigma\gamma\right)\sin^2\phi\right] E_x \\ &\quad + \varepsilon_0 \left[\left(\omega^2 - \jmath\omega\gamma - \omega_p^2\right) - \left(\varepsilon_\phi\omega^2 - \jmath\omega(\sigma + \varepsilon_\phi\gamma) - \sigma\gamma\right)\right] \\ &\quad \times \sin\phi\cos\phi E_y \\ &\quad = (\omega^2 - \jmath\omega\gamma)D_x. \end{aligned} \tag{16}$$

The updating dispersive FDTD equation was obtained from (16) via the inverse Fourier transform ($\jmath\omega \rightarrow (\partial/\partial t)$, $\omega^2 \rightarrow -(\partial^2/\partial t^2)$), giving

$$\begin{aligned} &\varepsilon_0 \left[\left(\frac{\partial^2}{\partial t^2} + \gamma\frac{\partial}{\partial t} + \omega_p^2\right)\cos^2\phi \right. \\ &\quad \left. + \left(\varepsilon_\phi\frac{\partial^2}{\partial t^2} + (\sigma + \varepsilon_\phi\gamma)\frac{\partial}{\partial t} + \sigma\gamma\right)\sin^2\phi\right] E_x \\ &\quad + \varepsilon_0 \left[\left(\frac{\partial^2}{\partial t^2} + \gamma\frac{\partial}{\partial t} + \omega_p^2\right)\right. \\ &\qquad \left. - \left(\varepsilon_\phi\frac{\partial^2}{\partial t^2} + (\sigma + \varepsilon_\phi\gamma)\frac{\partial}{\partial t} + \sigma\gamma\right)\right]\sin\phi\cos\phi E_y \\ &\quad = \left(\frac{\partial^2}{\partial t^2} + \gamma\frac{\partial}{\partial t}\right) D_x. \end{aligned} \tag{17}$$

A second-order discretization procedure was applied in (17), where the central finite difference operators in time (δ_t and δ_t^2) and the central average operators with respect to time (μ_t and μ_t^2) were used

$$\frac{\partial^2}{\partial t^2} \rightarrow \frac{\delta_t^2}{\Delta t^2}, \quad \frac{\partial}{\partial t} \rightarrow \frac{\delta_t}{\Delta t}\mu_t, \quad \omega_p^2 \rightarrow \omega_p^2\mu_t^2, \quad \sigma\gamma \rightarrow \sigma\gamma\mu_t^2 \tag{18}$$

where the operators $\delta_t, \delta_t^2, \mu_t, \mu_t^2$ are explained in [39] and given by

$$\begin{aligned} \delta_t F|_{i,j,k}^n &\equiv F|_{i,j,k}^{n+\frac{1}{2}} - F|_{i,j,k}^{n-\frac{1}{2}} \\ \delta_t^2 F|_{i,j,k}^n &\equiv F|_{i,j,k}^{n+1} - 2F|_{i,j,k}^n + F|_{i,j,k}^{n-1} \\ \mu_t F|_{i,j,k}^n &\equiv \frac{F|_{i,j,k}^{n+\frac{1}{2}} + F|_{i,j,k}^{n-\frac{1}{2}}}{2} \\ \mu_t^2 F|_{i,j,k}^n &\equiv \frac{F|_{i,j,k}^{n+1} + 2F|_{i,j,k}^n + F|_{i,j,k}^{n-1}}{4} \end{aligned} \tag{19}$$

where F represents arbitrary field components and (i,j,k) indices are the coordinates of a certain mesh point in the FDTD domain. Hence, the discretized (17) becomes

$$\begin{aligned} &\varepsilon_0\left[\left(\frac{\delta_t^2}{\Delta t^2} + \gamma\frac{\delta_t}{\Delta t} + \omega_p^2\mu_t^2\right)\cos^2\phi \right. \\ &\quad \left. + \left(\varepsilon_\phi\frac{\delta_t^2}{\Delta t^2} + (\sigma + \varepsilon_\phi\gamma)\frac{\delta_t}{\Delta t} + \sigma\gamma\mu_t^2\right)\sin^2\phi\right] E_x \\ &\quad + \varepsilon_0\left[\left(\frac{\delta_t^2}{\Delta t^2} + \gamma\frac{\delta_t}{\Delta t} + \omega_p^2\mu_t^2\right)\right. \\ &\qquad \left. - \left(\varepsilon_\phi\frac{\delta_t^2}{\Delta t^2} + (\sigma + \varepsilon_\phi\gamma)\frac{\delta_t}{\Delta t} + \sigma\gamma\mu_t^2\right)\right]\sin\phi\cos\phi E_y \\ &\quad = \left(\frac{\delta_t^2}{\Delta t^2} + \gamma\frac{\delta_t}{\Delta t}\right) D_x. \end{aligned} \tag{20}$$

Note that ε_ϕ remains constant in (20), because it is always greater than one, as with conventional dielectric materials. Finally, the operators (19) are substituted in (20) and the derived dispersive updating FDTD equation is

$$\begin{aligned} E_x^{n+1} = \left[C_1 D_x^{n+1} - B_1 E_y^{n+1} - C_2 D_x^n + A_2 E_x^n + B_2 E_y^n \right. \\ \left. + C_3 D_x^{n-1} - A_3 E_x^{n-1} - B_3 E_y^{n-1}\right]/A_1. \end{aligned} \tag{21}$$

With exactly the same procedure, the updating FDTD equation for the E_y component was derived from the second equation of (14) as

$$\begin{aligned} E_y^{n+1} = \left[C_1 D_y^{n+1} - B_1 E_x^{n+1} - C_2 D_y^n + F_2 E_y^n + B_2 E_x^n \right. \\ \left. + C_3 D_y^{n-1} - F_3 E_y^{n-1} - B_3 E_x^{n-1}\right]/F_1. \end{aligned} \tag{22}$$

The coefficients for both (21) and (22) are given by

$$A_1 = \frac{(\cos^2\phi + \varepsilon_\phi \sin^2\phi)}{\Delta t^2} + \frac{\omega_p^2 \cos^2\phi + \sigma\gamma \sin^2\phi}{4} + \frac{\gamma\cos^2\phi + (\sigma + \varepsilon_\phi\gamma)\sin^2\phi}{2\Delta t}$$

$$A_2 = \frac{2(\cos^2\phi + \varepsilon_\phi \sin^2\phi)}{\Delta t^2} - \frac{\omega_p^2 \cos^2\phi + \sigma\gamma \sin^2\phi}{2}$$

$$A_3 = \frac{(\cos^2\phi + \varepsilon_\phi \sin^2\phi)}{\Delta t^2} + \frac{\omega_p^2 \cos^2\phi + \sigma\gamma \sin^2\phi}{4} - \frac{\gamma\cos^2\phi + (\sigma + \varepsilon_\phi\gamma)\sin^2\phi}{2\Delta t}$$

$$B_1 = \frac{(1-\varepsilon_\phi)\sin\phi\cos\phi}{\Delta t^2} + \frac{\left(\omega_p^2 - \sigma\gamma\right)\sin\phi\cos\phi}{4} + \frac{(\gamma - \sigma - \varepsilon_\phi\gamma)\sin\phi\cos\phi}{2\Delta t}$$

$$B_2 = \frac{2(1-\varepsilon_\phi)\sin\phi\cos\phi}{\Delta t^2} - \frac{\left(\omega_p^2 - \sigma\gamma\right)\sin\phi\cos\phi}{2}$$

$$B_3 = \frac{(1-\varepsilon_\phi)\sin\phi\cos\phi}{\Delta t^2} + \frac{\left(\omega_p^2 - \sigma\gamma\right)\sin\phi\cos\phi}{4} - \frac{(\gamma - \sigma - \varepsilon_\phi\gamma)\sin\phi\cos\phi}{2\Delta t}$$

$$C_1 = \frac{1}{\varepsilon_0\Delta t^2} + \frac{\gamma}{2\varepsilon_0\Delta t},\ C_2 = \frac{2}{\varepsilon_0\Delta t^2}$$

$$C_3 = \frac{1}{\varepsilon_0\Delta t^2} - \frac{\gamma}{2\varepsilon_0\Delta t}$$

$$F_1 = \frac{(\sin^2\phi + \varepsilon_\phi \cos^2\phi)}{\Delta t^2} + \frac{\omega_p^2 \sin^2\phi + \sigma\gamma \cos^2\phi}{4} + \frac{\gamma\sin^2\phi + (\sigma + \varepsilon_\phi\gamma)\cos^2\phi}{2\Delta t}$$

$$F_2 = \frac{2(\sin^2\phi + \varepsilon_\phi \cos^2\phi)}{\Delta t^2} - \frac{\omega_p^2 \sin^2\phi + \sigma\gamma \cos^2\phi}{2}$$

$$F_3 = \frac{(\sin^2\phi + \varepsilon_\phi \cos^2\phi)}{\Delta t^2} + \frac{\omega_p^2 \sin^2\phi + \sigma\gamma \cos^2\phi}{4} - \frac{\gamma\sin^2\phi + (\sigma + \varepsilon_\phi\gamma)\cos^2\phi}{2\Delta t}$$

where Δt is the temporal discretization.

However, the (21) and (22) cannot be calculated with the FDTD algorithm. The reason is that, in the case of (21), the component E_y^{n+1} cannot be computed at the particular time step $(n+1)$. This also applies to the E_x^{n+1} component in (22). The solution is to substitute (22) into (21) and the inverse. As a result, the updating FDTD equation, which computes the E_x^{n+1} component, becomes

$$E_x^{n+1} = \Big[C_1 D_x^{n+1} - a_1 \overline{D}_y^{n+1} - C_2 D_x^n + a_2 \overline{D}_y^n + b_2 E_x^n + d_1 \overline{E}_y^n + C_3 D_x^{n-1} - a_3 \overline{D}_y^{n-1} - b_3 E_x^{n-1} - d_2 \overline{E}_y^{n-1}\Big]/b_1. \quad (23)$$

The updating FDTD equation for the E_y^{n+1} component was found, in exactly the same way, to be

$$E_y^{n+1} = \Big[C_1 D_y^{n+1} - e_1 \overline{D}_x^{n+1} - C_2 D_y^n + e_2 \overline{D}_x^n + f_2 E_y^n + g_1 \overline{E}_x^n + C_3 D_y^{n-1} - e_3 \overline{D}_x^{n-1} - f_3 E_y^{n-1} - g_2 \overline{E}_x^{n-1}\Big]/f_1 \quad (24)$$

where the newly introduced coefficients in (23) and (24) are

$$a_1 = \frac{B_1C_1}{F_1}, a_2 = \frac{B_1C_2}{F_1}, a_3 = \frac{B_1C_3}{F_1}$$

$$b_1 = A_1 - \frac{B_1^2}{F_1}, b_2 = A_2 - \frac{B_1B_2}{F_1}, b_3 = A_3 - \frac{B_1B_3}{F_1}$$

$$d_1 = B_2 - \frac{B_1F_2}{F_1}, d_2 = B_3 - \frac{B_1F_3}{F_1}$$

$$e_1 = \frac{B_1C_1}{A_1}, e_2 = \frac{B_1C_2}{A_1}, e_3 = \frac{B_1C_3}{A_1}$$

$$f_1 = F_1 - \frac{B_1^2}{A_1}, f_2 = F_2 - \frac{B_1B_2}{A_1}, f_3 = F_3 - \frac{B_1B_3}{A_1}$$

$$g_1 = B_2 - \frac{A_2B_1}{A_1}, g_2 = B_3 - \frac{A_3B_1}{A_1}.$$

For more accurate results, the overlined field components $\overline{D}_y$, $\overline{E}_y$, $\overline{D}_x$, $\overline{E}_x$ were calculated with a locally spatial averaging technique [40]. This method was employed because the x and y field components were located in different mesh points across the FDTD grid. Their averaged values were computed from [40]

$$\overline{E}_y(i,j) = [E_y(i,j) + E_y(i+1,j) + E_y(i,j-1) + E_y(i+1,j-1)]/4 \quad (25)$$

where (i,j) are the coordinates of the mesh point.

The final step was to introduce the updating FDTD equation of the H_z field component. From (7), the magnetic permeability μ_z component can have values both less and greater than one. Hence, a more complicated approach was necessary to model the magnetic field H_z component. When $\mu_z < 1$, the magnetic permeability was mapped with the Drude model, given by

$$\mu_z = 1 - \frac{\omega_{pm}^2}{\omega^2 - j\omega\gamma_m} \quad (26)$$

where ω_{pm} is the magnetic plasma frequency and γ_m is the magnetic collision frequency, which measures the losses of the magnetic dispersive material. The analytical equations of ω_{pm} and γ_m were derived in the same way as (9) and (10) and are given by

$$\omega_{pm}^2 = (1-\mu_z)\omega^2 + \mu_z\omega\gamma_m \tan\delta_m \quad (27)$$

$$\gamma_m = \frac{\mu_z\omega\tan\delta_m}{(1-\mu_z)}. \quad (28)$$

It can be seen from the above (27) and (28), that the magnetic plasma and collision frequencies are radially-dependent, because they are functions of μ_z, as given by (7).

Equation (26) was substituted in the constitutive equation (4), and it was discretized as in [38]. The updating FDTD equation for this case is

$$H_z^{n+1} = \left\{\left[\frac{1}{\mu_0\Delta t^2} + \frac{\gamma_m}{2\mu_0\Delta t}\right]B_z^{n+1} - \frac{2}{\mu_0\Delta t^2}B_z^n + \left[\frac{1}{\mu_0\Delta t^2} - \frac{\gamma_m}{2\mu_0\Delta t}\right]B_z^{n-1} + \left[\frac{2}{\Delta t^2} - \frac{\omega_{pm}^2}{2}\right]H_z^n - \left[\frac{1}{\Delta t^2} - \frac{\gamma_m}{2\Delta t} + \frac{\omega_{pm}^2}{4}\right]H_z^{n-1}\right\} \Bigg/ \left[\frac{1}{\Delta t^2} + \frac{\gamma_m}{2\Delta t} + \frac{\omega_{pm}^2}{4}\right]. \quad (29)$$

When the magnetic permeability of the cloaking material is $\mu_z \geq 1$, it was simulated with the conventional lossy magnetic model

$$\hat{\mu}_z = \mu_z + \frac{\sigma_m}{\jmath\omega} \tag{30}$$

where the component μ_z is radially-dependent and given by (7). The parameter σ_m is the magnetic conductivity. The loss tangent of the lossy magnetic material is given by $\tan\delta_m = \sigma_m/\omega\mu_z$ and it is also radially-dependent. The updating FDTD equation, for this type of material, is derived from the discrete Faraday law [see (5)] including the losses [37]. Finally, the updating FDTD equation, between H and E field components, was equal to the discrete Ampere law [see (6)] in free space.

Note that the method in [34], for the full set of cloaking parameters [see (7)], cannot be applied when $\varepsilon_r = 0$, which occurs only at the inner radius points of the cloaking device ($r = R_1$). More precisely, the permittivity tensor $\{\varepsilon\}$ (13) cannot be inverted when $\varepsilon_r = 0$, because its determinant is equal to: $|\varepsilon| = \varepsilon_r\varepsilon_\phi$. From (7), it was obtained that $\varepsilon_\phi \neq 0$ for all the radius values. Thus, for the case of $\varepsilon_r = 0$, the determinant $|\varepsilon|$ is zero and the array $\{\varepsilon\}$ cannot be inverted. Furthermore, for the method presented in [34], the conductive losses of the $\hat{\varepsilon}_\phi$ component and the conventional magnetic losses of the $\hat{\mu}_z$ parameter were not introduced in the updating FDTD equations. Therefore, the currently proposed FDTD method is an extension of the one proposed in [34] and it can also simulate lossy electromagnetic cloaks. The proposed method can easily be extended in order to model three dimensional (3-D) lossy electromagnetic cloaks.

Numerical approximations are inevitable, when the FDTD method is applied. Space and time are discretized, with a detrimental effect on the accuracy of the simulations. Furthermore, the permittivity and permeability are frequency-dependent, modeled with the Drude dispersion model (8), and the conventional lossy dielectric/magnetic behavior (11) is used. Due to the presence of a discrete time step Δt, which is always used in the FDTD method, there will be differences between the analytical and the numerical characteristics of the cloaking material. Hence, for the proposed dispersive FDTD method, a spatial resolution of $\Delta x < \lambda/10$ is insufficient, unlike the conventional dielectric material simulations, where it is the required value [37]. From a previous analysis of left-handed metamaterials [38], it was found that spurious resonances are caused by coarse time discretization, which directly leads to numerical errors and inaccurate modeling results. It was proposed that a spatial resolution of $\Delta x < \lambda/80$ is essential for accurate simulations. The same and more dense spatial resolution restrictions have to be applied in the simulation of the cloaking structure.

The same approach as that taken in [34] and [38] will be followed for the computation of the numerical values of the permittivities ε_r, ε_ϕ and the permeability μ_z. The plane waves, described in a discrete-time form, are

$$E^n = Ee^{\jmath n\omega\Delta t}, \quad D^n = De^{\jmath n\omega\Delta t}. \tag{31}$$

They are substituted in (21) and the calculated numerical permittivities $\widetilde{\varepsilon_r}, \widetilde{\varepsilon_\phi}$ are

$$\widetilde{\varepsilon_r} = \left[1 - \frac{\omega_p^2\Delta t^2\cos^2\frac{\omega\Delta t}{2}}{2\sin\frac{\omega\Delta t}{2}\left(2\sin\frac{\omega\Delta t}{2} - \jmath\gamma\Delta t\cos\frac{\omega\Delta t}{2}\right)}\right] \tag{32}$$

$$\widetilde{\varepsilon_\phi} = \varepsilon_\phi + \frac{\sigma\Delta t}{2\jmath\tan\frac{\omega\Delta t}{2}}. \tag{33}$$

Notice that, when $\Delta t \to 0$, which leads to a very fine FDTD grid, the (32) and (33) are transformed to the Drude model (8) and the lossy dielectric material (11), respectively. Exactly the same numerical permeability $\widetilde{\mu_z}$ formulas can be produced for the dispersive magnetic model (26) and the conventional lossy magnetic material (30). The comparison between analytic and numerical material parameters is given in [34]. It is concluded that conventional spatial resolutions with values $\Delta x < \lambda/10$ are not appropriate for this kind of anisotropic material and more fine FDTD meshes, with $\Delta x < \lambda/80$, have to be applied to maintain the simulation accuracy.

Another problem, which was dominant during the FDTD modeling of cloaking structure, was numerical instability. The Courant stability criterion $\Delta t = \Delta x/\sqrt{2}c$ [37] was satisfied during the FDTD simulations. The object, which was "cloaked," was chosen to be composed of a perfect electric conductor (PEC) material. Arbitrary materials can be used for the object placed inside the cloaking shell. However, for FDTD modeling, it is better to choose the PEC material, because very small field values will always be expected inside the cloaked space. This is due to the numerical approximations, which are inherent to the FDTD method. The instability was generated at two specific regions of the cloaking FDTD meshes. The first instability region was obtained at the interface between the cloaking material and free space ($r = R_2$). The other was concentrated at the interface between the cloaking device and the "cloaked" PEC material ($r = R_1$). In both regions, the permittivities ε_r, ε_ϕ and the permeability μ_z are changing rapidly from finite, even zero, to infinite theoretical values. As a result, spurious cavity resonances are created, which are combined with the irregular staircase approximation of the cloaking structure's cylindrical geometry. From the discretization, with the FDTD method, of the divergence of the electric flux density $\nabla \cdot D$, it can be concluded that the instability is present in the form of accumulated charges at these two interfaces.

In order to achieve stable FDTD simulations, a series of modifications was applied in the conventional FDTD algorithm. First, the locally spatial averaging technique (25) was introduced for the simulation of the constitutive equation, which is given in tensor form in (13). This method improved the stability and accuracy of the cloaking modeling. Fine spatial resolutions ($\Delta x < \lambda/80$) were applied, which alleviated the effect of the inevitable—for the current cylindrical geometry—staircase approximation. Ideally, an infinite spatial resolution will guarantee an accurate and stable cloaking modeling. Moreover, there are differences between the analytical and the numerical [see (32)] material parameters, which affected the stability of the FDTD simulations in a straightforward manner. Corrected numerical electric and magnetic plasma and collision frequencies were computed. The required numerical lossy permittivity was equal

to $\widetilde{\varepsilon_r} = \varepsilon_r(1 - j\tan\delta)$, where ε_r was radially-dependent (7) and $\tan\delta$ was the loss tangent of the cloaking material. If the numerical lossy permittivity is substituted in (32), the resulting corrected plasma and collision frequencies were obtained as [34]

$$\widetilde{\omega}_p^2 = \frac{2\sin\frac{\omega\Delta t}{2}\left[-2(\varepsilon_r - 1)\sin\frac{\omega\Delta t}{2} + \varepsilon_r\gamma\Delta t\cos\frac{\omega\Delta t}{2}\tan\delta\right]}{\Delta t^2\cos^2\frac{\omega\Delta t}{2}} \tag{34}$$

$$\widetilde{\gamma} = \frac{2\varepsilon_r\sin\frac{\omega\Delta t}{2}\tan\delta}{(1-\varepsilon_r)\Delta t\cos\frac{\omega\Delta t}{2}}. \tag{35}$$

For the conventional lossy dielectric/magnetic model, the only correction, for improved stability, was applied at the frequency ω. The corrected frequency was easily obtained from (33)

$$\widetilde{\omega} = \frac{\tan\frac{\omega\Delta t}{2}}{\Delta t/2}. \tag{36}$$

With all the previous modifications, a stable FDTD simulation can be satisfied at the outer interface $(r = R_2)$ of the cloaking structure. For the inner interface $(r = R_1)$, one more modification has to be applied in the FDTD algorithm, in order to achieve stability. The correct definition of the "cloaked" perfect electric conductor (PEC) material is crucial for stable modeling of the cloak. The PEC is defined in the FDTD code as a material with infinite permittivity $(\varepsilon \to \infty)$. Hence, the coefficient $(\Delta t/\varepsilon)$, in the discrete Ampere's law [see (6)], has to be set to zero inside the PEC material, in order to achieve a correct and stable simulation. After all these modifications, which have been made to the FDTD algorithm, the resulted modeling is stable and the numerical accuracy has been improved. There are no accumulated charges at the two interfaces $(r = R_1, r = R_2)$, which is evident by the FDTD simulation of the divergence of the electric flux density $\nabla \cdot D$.

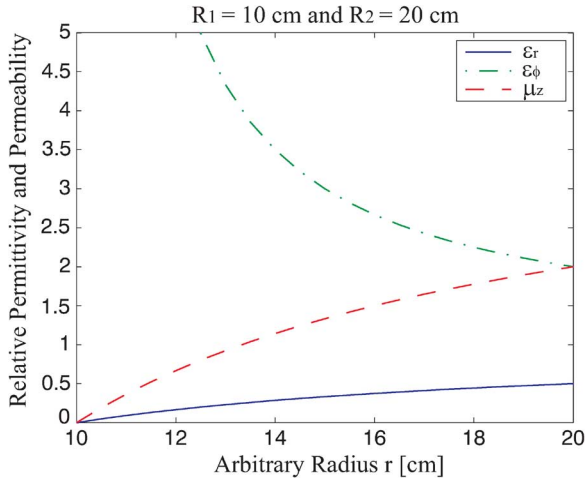

Fig. 1. The full set of cloaking material parameters used in the FDTD simulation.

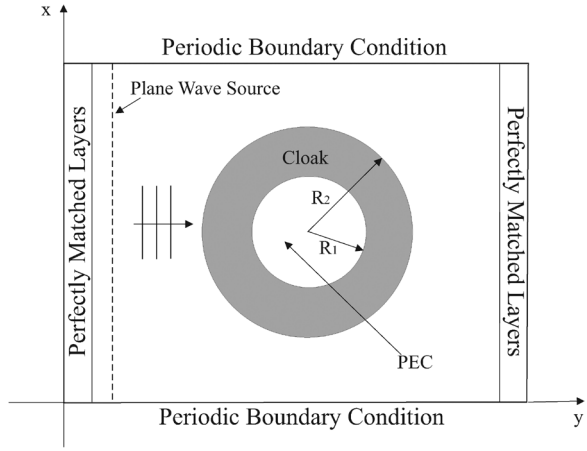

Fig. 2. A 2-D FDTD computation domain of the cloaking structure for the case of plane wave excitation.

III. Numerical Results

A TE polarized plane wave source was utilized to illuminate the 2-D FDTD-modeled cloaking structure. A uniform spatial discretization was used, with an FDTD cell size of $\Delta x = \Delta y = \lambda/150$, where λ is the wavelength of the excitation signal. In this case, the operating frequency was $f = 2$ GHz and the free space wavelength was $\lambda = 15$ cm. The temporal discretization was chosen according to the Courant stability condition [37] and the time step was given by $\Delta t = \Delta x/\sqrt{2}c$, where c is the speed of light in free space.

First, the lossless cloaking shell was simulated to validate the proposed FDTD method, which meant that the collision frequency in the Drude model (8) was equal to zero $(\gamma = 0)$. Furthermore, the conductivity in (11) is set to zero $(\sigma = 0)$. Hence, the radially-dependent plasma frequency was computed from the simplified equation $\omega_p = \omega\sqrt{1-\varepsilon_r}$, where ε_r is given by (7). The inner and outer radius—of the cloaking device—had dimensions $R_1 = 10$ cm and $R_2 = 20$ cm, respectively. The full set of the cloaking parameters [see (7)] is changing with the cloak's radius, as shown in Fig. 1. The computational domain was terminated along the y-direction with Berenger's perfectly matched layers (PMLs) [41]. The waves were fully absorbed in the PMLs, equivalent to their leaving the computation domain without introducing reflections. In the last layer of the computational domain along the x-direction, Bloch's periodic boundary conditions (PBCs) [37] were applied, in order to create a propagating plane wave. The FDTD computation domain for the current simulations is shown in Fig. 2. The results for plane wave excitation, when the steady-state is reached, are given in Fig. 3. A transverse profile of the propagating field in the lossless cloaking shell is depicted in Fig. 4.

In Fig. 3, the electromagnetic wave propagates from left to right in the FDTD computation domain. The wave bends inside the cloaking device in order to avoid the "cloaked" object, as was expected. The wave trajectory is recomposed without any disturbance behind the cloaking shell. Therefore, the object placed inside the cloaking structure appears as if it does not exist, like it is "invisible." Note that, for this type of cloaking device, there are no constraints about the size and the material type of the "hidden" object. This is in contrast to the properties of the proposed plasmonic and LHM-based cloaking devices [42]–[45]. In Fig. 3, a small disturbance of the plane wave is visible leaving the cloak on the right-hand side. Furthermore, there is a slight scattering coming back to the source plane on the left-hand side. The reason is that the surface of the cloaking device

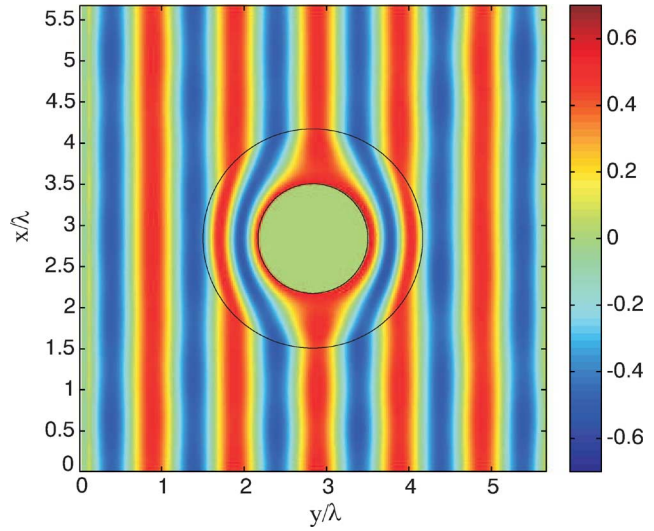

Fig. 3. Normalized magnetic field distribution of the lossless cloaking device with plane wave excitation. The wave propagates from left to right and the cloaked object is composed of PEC material.

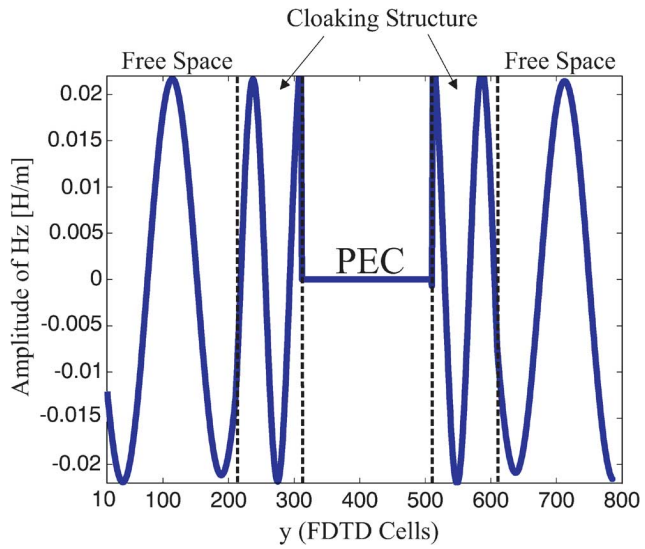

Fig. 4. A transverse profile of the magnetic field H_z component propagating through the lossless cloaking device. The wave propagates from left to right undisturbed.

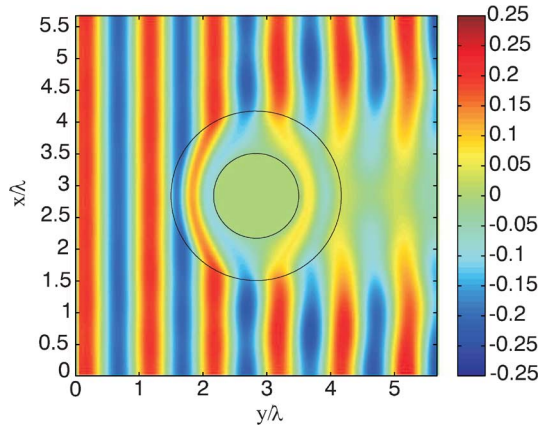

Fig. 5. Normalized magnetic field distribution of the lossy cloaking device with plane wave excitation. Ideal parameters are used with a loss tangent of 0.1. The wave propagates from left to right and the cloaked object is composed of PEC material.

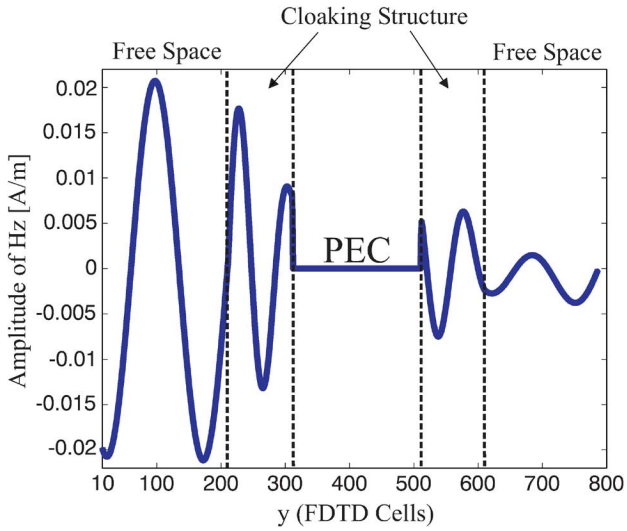

Fig. 6. Magnetic field H_z component propagating through the lossy cloaking device ($\tan\delta = 0.1$). The wave propagates from left to right and it is dissipated at the right side of the cloak.

is curved (cylindrical structure), but it is being modeled with a Cartesian FDTD mesh. As a result, a staircase approximation is inevitable, which directly reduces the simulation accuracy. This problem can be solved if a conformal scheme [46] is utilized or a cylindrical FDTD is applied, combined with a dispersive FDTD scheme. However, the analysis of the conformal dispersive FDTD [46] technique leads to a complicated sixth-order differential equation for the simulation of the cloaking structure. This is due to the anisotropy of the cloaking material parameters.

The next step was to introduce losses in the radially-dependent and dispersive cloaking material, which is a far more practical and realistic representation of the metamaterials. The loss tangent, $\tan\delta$, was set equal to 0.1, for both the dispersive ε_r component [see (8)] and the conventional lossy dielectric component $\hat{\varepsilon}_\phi$ [(11)]. For the magnetic component μ_z, the magnetic loss tangent is chosen to be $\tan\delta_m = 0.1$, again for both the dispersive [see (26)] and the conventional lossy [see (30)] cases. The FDTD computational domain scenario used to simulate the lossy cloak is the same as in Fig. 2. The magnetic field H_z distribution, with a plane wave excitation, is depicted in Fig. 5. It is observed that the cloaking device is working (bending of waves) properly, like the lossless case. But, due to the presence of losses in electromagnetic cloaks, there is a strong shadowing effect to the field behind the cloaking shell. The attenuation of the propagating magnetic field H_z component through the lossy cloak is clearly depicted in Fig. 6. For $\tan\delta = 0.01$, the magnetic field pattern is almost identical to the ideal lossless case in Fig. 3. However, the cloaking performance is impaired due to the shadow cast behind the cloaked object, for a loss tangent of $\tan\delta = 0.1$. Therefore, the proposed cloaking structure is sensitive to losses, which is a drawback towards the realization of future "invisibility" devices.

The scattering coefficients of lossless and lossy cloaks are calculated with reference to the free space case, with no obstacles

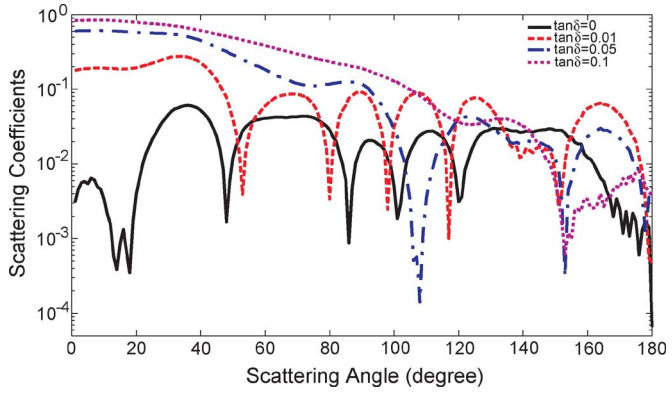

Fig. 7. Scattering patterns of lossless and lossy cloaks. Equal loss tangents of the electric and magnetic parameters were chosen, which range from 0 to 0.1.

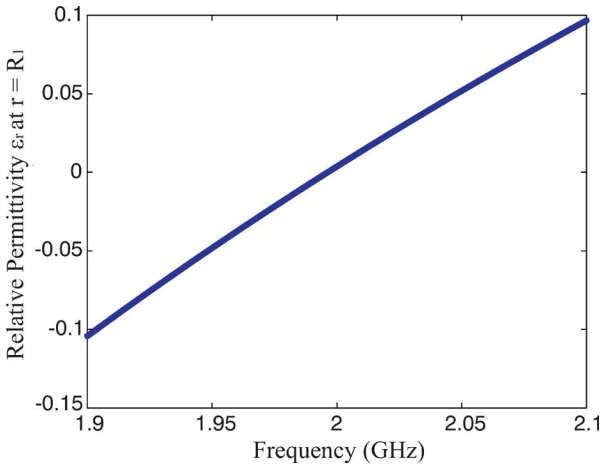

Fig. 8. Ideal cloaking material parameter ε_r, at the point $r = R_1$ of the cloak, varying with the frequency. Note that the values of ε_r are always less than one and they can be negative.

present. Equal loss values are chosen for the electric permittivities ε_r, ε_ϕ and the permeability μ_z components $(\tan\delta = \tan\delta_m)$. The scattering patterns, varying with the losses, are depicted in Fig. 7, where the angles of 0° and 180° are forward and backward scattering, respectively. It is interesting to compare our numerical results of Fig. 7 with the analytical computed far-field scattering performance of the cylindrical cloak presented in [32]. It is seen that the scattering coefficients increase with the losses; furthermore the minimum scattering is no longer at the backscattering point (angle of 180°) as the losses rise, which is in good agreement with the analytical solution of the cloak [32].

The losses directly affect the cloak's performance; moreover the cloaking material parameters are frequency-dispersive. For example, it is seen in Fig. 8 how the value of ε_r at the inner radius of the cloaking device $(r = R_1)$ is changing with a slight deviation from the center frequency of 2 GHz. Hence, the cloak is functional only at a narrow frequency range. The FDTD method gives us the flexibility to easily perceive the bandwidth issues of the cloaking device, because it is a time-domain numerical technique. FDTD modeling of the lossless cloaking device will again be employed to investigate the bandwidth limitations of the cloak. The computation domain is the same as in

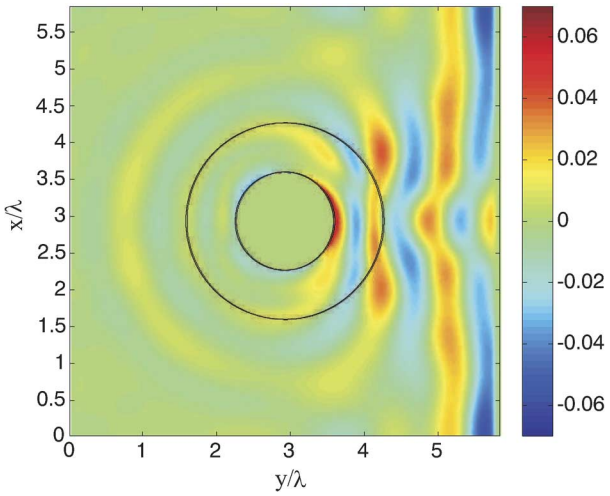

Fig. 9. A wideband Gaussian pulse propagating from the left to the right side of the cloak. The pulse has a fixed bandwidth between 1–3 GHz, centered at a frequency of 2 GHz. The snapshot is taken when the pulse is recomposed at the right side of the cloak.

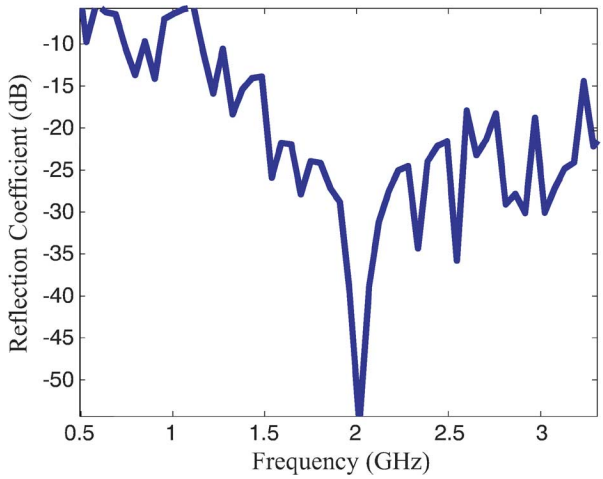

Fig. 10. Reflection coefficient of cloak in dB, varying with frequency. The device is illuminated with a wideband Gaussian pulse.

Fig. 2 and the updating FDTD equations are given by (5), (6), (23), (24), and (29). The excitation of this simulation is a wideband Gaussian pulse with a fixed bandwidth between 1–3 GHz, centered at a frequency of 2 GHz.

The wideband Gaussian pulse is shown in Fig. 9 after it has propagated through the cloaking device. It is obvious that there are reflections and that the pulse trajectory is not recomposed correctly. However, the bending of the electromagnetic pulse inside the device is similar to that seen when using the ideal cloak. Recently, an interesting bandwidth study of the spherical cloak, using the analytical Mie scattering model, was published [47]. Here, the reflection coefficient of the cloaking device was calculated, in order to measure the backscatter of the structure. The magnetic field values H_z are averaged along a parallel to the x-axis line, close to the plane wave source and the excitation pulse is isolated from the reflected signal. Furthermore, the transmission coefficient was measured with the same technique of averaging the field values along a line, close to

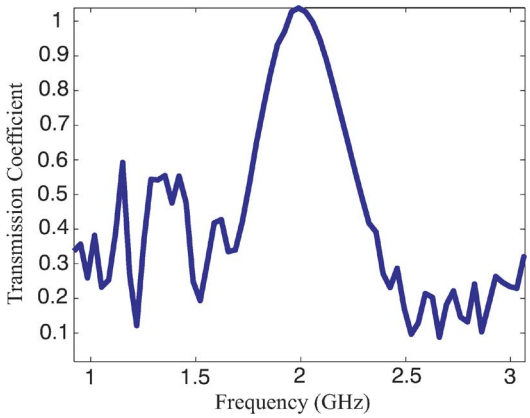

Fig. 11. Transmission coefficient of cloak, varying with frequency. The device is illuminated with a wideband Gaussian pulse.

the right side PML wall. The computed reflection and transmission coefficients can be seen in Figs. 10 and 11, respectively. To conclude, the cloak has acceptable performance over a narrow bandwidth only, with ideal behavior (no reflections and total transmission of the field) at one frequency, namely the center frequency (2 GHz). However, it is interesting that the device can operate with a tolerable percentage of reflections and a half fraction of transmitted signal in a wider frequency range.

IV. Conclusion

In this paper, a novel radially-dependent dispersive FDTD technique was proposed to model a lossy cloaking device. The cloaking material parameters were mapped to the dispersive Drude model and the constitutive equations were discretized in space and time. Both lossless and lossy electromagnetic cloaks was investigated. The FDTD simulation results were in good agreement with similar findings from the theoretical analysis and the frequency domain numerical modeling of the cloaking structure. From the FDTD numerical modeling, it was concluded that the cloaking structure is sensitive to losses. Moreover, it can be perfectly "invisible" only at a very narrow frequency range. However, it would be very interesting to study how lossy cloaks behave over a wide frequency range. The proposed FDTD technique can be easily extended to simulate 3-D cloaking structures. Nevertheless, fine spatial resolutions (at least $\lambda/80$) must be used to achieve stable and accurate results; this is not a major factor for 2-D simulations, but would be a serious concern for middle-to-large sized real-life 3-D cloaking devices. This problem can be faced with the utilization of conformal FDTD methods and/or parallel programming techniques operating at powerful computer cluster facilities. Finally, note that novel microwave absorbers and antenna structures may be developed based on the general concept of coordinate transformation used in electromagnetic cloaking.

Acknowledgment

The authors would like to thank Dr. R. Foster for his help during the preparation of the manuscript.

References

[1] J. B. Pendry, D. Schurig, and D. R. Smith, "Controlling electromagnetic fields," *Science*, vol. 312, pp. 1780–1782, 2006.
[2] U. Leonhardt, "Optical conformal mapping," *Science*, vol. 312, p. 17771780, 2006.
[3] U. Leonhardt, "Notes on conformal invisibility devices," *New Jour. Physics 8*, vol. 118, 2006.
[4] V. G. Veselago, "The electrodynamics of substances with simultaneously negative values of ε and μ," *Sov. Phys. Usp.*, vol. 10, pp. 509–514, 1968.
[5] S. A. Cummer, B.-I. Popa, D. Schurig, D. R. Smith, and J. B. Pendry, "Full-wave simulations of electromagnetic cloaking structures," *Phys. Rev. E*, vol. 74, p. 036621, 2006.
[6] W. Cai, U. K. Chettiar, A. V. Kildishev, and V. M. Shalaev, "Optical cloaking with metamaterials," *Nat. Photon.*, vol. 1, p. 224227, 2007.
[7] M. Yan, Z. Ruan, and M. Qiu, "Scattering characteristics of simplified cylindrical invisibility cloaks," *Opt. Express*, vol. 15, no. 26, pp. 17772–17782, 2007.
[8] D. Schurig, J. J. Mock, B. J. Justice, S. A. Cummer, J. B. Pendry, A. F. Starr, and D. R. Smith, "Metamaterial electromagnetic cloak at microwave frequencies," *Science*, vol. 314, p. 977980, 2006.
[9] I. Smolyaninov, Y. Hung, and C. Davis, "Two-dimensional metamaterial structure exhibiting reduced visibility at 500 nm," *Opt. Lett.s*, vol. 33, pp. 1342–1344, 2008.
[10] W. Cai, U. K. Chettiar, A. V. Kildishev, V. M. Shalaev, and G. W. Milton, "Nonmagnetic cloak with minimized scattering," *Appl. Phys. Lett.*, vol. 91, p. 111105, 2007.
[11] W. Cai, U. K. Chettiar, A. V. Kildishev, and V. M. Shalaev, "Designs for optical cloaking with high-order transformations," *Opt. Express*, vol. 16, no. 8, pp. 5444–5452, 2008.
[12] H. Chen, Z. Liang, P. Yao, X. Jiang, H. Ma, and C. T. Chan, "Extending the bandwidth of electromagnetic cloaks," *Phys. Rev. B*, vol. 76, p. 241104, 2007.
[13] P. Yao, Z. Liang, and X. Jiang, "Limitation of the electromagnetic cloak with dispersive material," *Appl. Phys. Lett.*, vol. 92, p. 031111, 2008.
[14] E. Wolf and T. Habashy, "Invisible bodies and uniqueness of the inverse scattering problem," *J. Mod. Opt.*, vol. 40, pp. 785–792, 1993.
[15] Y. Huang, Y. Feng, and T. Jiang, "Electromagnetic cloaking by layered structure of homogeneous isotropic materials," *Opt. Express*, vol. 15, no. 18, pp. 11133–11141, 2007.
[16] D. A. B. Miller, "On perfect cloaking," *Opt. Express*, vol. 14, no. 25, pp. 12457–12466, 2006.
[17] P.-S. Kildal, "Artificially soft and hard surfaces in electromagnetics," *IEEE Trans. Antennas Propag.*, vol. 38, pp. 1537–1544, Oct. 1990.
[18] P.-S. Kildal, A. Kishk, and A. Tengs, "Reduction of forward scattering from cylindrical objects using hard surfaces," *IEEE Trans. Antennas Propag.*, vol. 44, pp. 1509–1520, 1996.
[19] A. Greenleaf, Y. Kurylev, M. Lassas, and G. Uhlmann, "Improvement of cylindrical cloaking with the SHS lining," *Opt. Express*, vol. 15, no. 20, pp. 12717–12734, 2007.
[20] D.-H. Kwon and D. H. Werner, "Two-dimensional eccentric elliptic electromagnetic cloaks," *Appl. Phys. Lett.*, vol. 92, p. 013505, 2008.
[21] M. Rahm, D. Schurig, D. A. Roberts, S. A. Cummer, D. R. Smith, and J. B. Pendry, "Design of electromagnetic cloaks and concentrators using form-invariant coordinate transformations of Maxwell's equations," *Phot. Nanostr.—Fund. Appl.*, vol. 6, p. 8795, 2008.
[22] S. A. Cummer and D. Schurig, "One path to acoustic cloaking," *New J. Phys.*, vol. 45, 2007.
[23] H. Chen and C. T. Chan, "Acoustic cloaking in three dimensions using acoustic metamaterials," *Appl. Phys. Lett.*, vol. 91, p. 183518, 2007.
[24] D. Schurig, J. B. Pendry, and D. R. Smith, "Transformation-designed optical elements," *Opt. Express*, vol. 15, no. 22, pp. 14772–14782, 2007.
[25] M. Tsang and D. Psaltis, "Magnifying perfect lens and superlens design by coordinate transformation," *Phys. Rev. B*, vol. 77, p. 035122, 2008.
[26] H. Chen and C. T. Chan, "Transformation media that rotate electromagnetic fields," *Appl. Phys. Lett.*, vol. 90, p. 241105, 2007.
[27] Y. Luo, J. Zhang, L. Ran, H. Chen, and J. A. Kong, "Controlling the emission of electromagnetic sources by coordinate transformation," ArXiv.org:0712.3776v1, 2007.
[28] M. Rahm, S. A. Cummer, D. Schurig, J. B. Pendry, and D. R. Smith, "Optical design of reflectionless complex media by finite embedded coordinate transformations," *Phys. Rev. Lett.*, vol. 100, p. 063903, 2008.
[29] D. Schurig, J. B. Pendry, and D. R. Smith, "Calculation of material properties and ray tracing in transformation media," *Opt. Express*, vol. 14, no. 21, pp. 9794–9804, 2006.

[30] Z. Ruan, M. Yan, C. W. Neff, and M. Qiu, "Ideal cylindrical cloak: Perfect but sensitive to tiny perturbations," *Phys. Rev. Lett.*, vol. 99, p. 113903, 2007.
[31] H. Chen, B.-I. Wu, B. Zhang, and J. A. Kong, "Electromagnetic wave interactions with a metamaterial cloak," *Phys. Rev. Lett.*, vol. 99, p. 063903, 2007.
[32] B. Zhang, H. Chen, B.-I. Wu, Y. Luo, L. Ran, and J. A. Kong, "Response of a cylindrical invisibility cloak to electromagnetic waves," *Phys. Rev. B*, vol. 76, p. 121101R, 2007.
[33] R. Weder, "Rigorous analysis of high-order electromagnetic invisibility cloaks," *J. Phys. A: Math. Theor.*, vol. 41, p. 065207, 2008.
[34] Y. Zhao, C. Argyropoulos, and Y. Hao, "Full-wave finite-difference time-domain simulation of electromagnetic cloaking structures," *Opt. Express*, vol. 16, no. 9, pp. 6717–6730, 2008.
[35] Z. Liang, P. Yao, X. Sun, and X. Jiang, "The physical picture and the essential elements of the dynamical process for dispersive cloaking structures," *Appl. Phys. Lett.*, vol. 92, p. 131118, 2008.
[36] O. P. Gandhi, B.-Q. Gao, and J.-Y. Chen, "A frequency-dependent finite-difference time-domain formulation for general dispersive media," *IEEE Trans. Microw. Theory Tech.*, vol. 41, p. 658665, 1993.
[37] A. Taflove and S. C. Hagness, *Computational Electrodynamics: The Finite-Difference Time-Domain Method*, 3rd ed. : Artech House, 2005.
[38] Y. Zhao, P. Belov, and Y. Hao, "Accurate modelling of left-handed metamaterials using a finite-difference time-domain method with spatial averaging at the boundaries," *Jour. Opt. A: Pure Appl. Opt.*, vol. 9, pp. 468–475, 2007.
[39] F. B. Hildebrand, *Introduction to Numerical Analysis*. New York: Mc-Graw-Hill, 1956.
[40] J.-Y. Lee and N.-H. Myung, "Locally tensor conformal FDTD method for modelling arbitrary dielectric surfaces," *Microw. Opt. Tech. Lett.*, vol. 23, pp. 245–249, 1999.
[41] J.-P. Bérenger, "A perfectly matched layer for the absorption of electromagnetic waves," *J. Comp. Phys.*, vol. 114, pp. 185–200, 1994.
[42] A. Alu and N. Engheta, "Achieving transparency with plasmonic and metamaterial coatings," *Phys. Rev. E*, vol. 72, p. 016623, 2005.
[43] G. W. Milton and N. P. Nicorovici, "On the cloaking effects associated with anomalous localized resonance," *Proc. R. Soc. A*, vol. 462, pp. 3027–3059, 2006.
[44] F. J. G. de Abajo, G. Gomez-Santos, L. A. Blanco, A. G. Borisov, and S. V. Shabanov, "Tunneling mechanism of light transmission through metallic films," *Phys. Rev. Lett.*, vol. 95, p. 067403, 2005.
[45] H. Cory, Y. Lee, Y. Hao, and C. Parini, "Use of conjugate dielectric and metamaterial slabs as radomes," *IET Microw. Antenna Propag.*, vol. 1, pp. 137–143, 2007.
[46] Y. Zhao and Y. Hao, "Finite-difference time-domain study of guided modes in nano-plasmonic waveguides," *IEEE Trans. Antennas Propag.*, vol. 55, pp. 3070–3077, 2007.
[47] B. Zhang, B. Wu, H. Chen, and J. Kong, "Rainbow and blueshift effect of a dispersive spherical invisibility cloak impinged on by a non-monochromatic plane wave," *Phys. Rev. Lett.*, vol. 101, p. 63902, 2008.

Christos Argyropoulos (S'04) received the Diploma of Electrical and Computer Engineering from the Aristotle University of Thessaloniki, Thessaloniki, Greece, in 2006, and the M.Sc. degree in communication engineering from the University of Manchester, Manchester, U.K., in 2007. He is currently working toward the Ph.D. degree at Queen Mary, University of London, U.K.

His main research interests include computational electromagnetics, numerical and analytical modeling of metamaterials and their applications, Antennas design and UWB systems. He has published and presented many papers in a number of established international conferences.

Yan Zhao (S'03–M'08) received the B.Sc. degree from Beijing University of Posts and Telecommunications (BUPT), Beijing, China, in 2002, the M.Sc. degree from the University of Birmingham, Birmingham, U.K., in 2003, and the Ph.D. degree from Queen Mary, University of London, London, U.K., in 2007.

He is currently a Research Assistant in The Antennas and Electromagnetics Group, School of Electronic Engineering and Computer Science, Queen Mary, University of London. He has published over 40 technical papers in highly ranked journals and refereed conference proceedings. Some of the papers have been published in *Optics Express, Physical Review E, Applied Physics Letters, Journal of Optics A*, the IEEE TRANSACTIONS and IEEE LETTERS. He has more than six years' experience in computational electromagnetics, notably in the area of finite-difference time-domain (FDTD) method for metamaterials. He also has experience with the ray tracing technique, the geometrical theory of diffraction (GTD), the uniform theory of diffraction (UTD) and their applications in antenna engineering and radio propagation.

Dr. Zhao has served as a reviewer for *Optics Express*, the IEEE TRANSACTIONS ON ANTENNAS AND PROPAGATION, *IEEE Microwave and Wireless Component Letters*, *Journal of Electromagnetic Waves and Applications* (JEMWA), and *International Journal of Infrared and Millimeter Waves*.

Yang Hao (M'00–SM'06), received the Ph.D. degree from the Centre for Communications Research (CCR), University of Bristol, Bristol, U.K., in 1998.

From 1998 to 2000, he was a Postdoctoral Research Fellow with the School of Electrical and Electronic Engineering, University of Birmingham, U.K. In May 2000, he joined the Antenna Engineering Group, Queen Mary College, University of London, London, U.K., first as a Lecturer and was promoted to Reader in 2005, and Professor in 2007. He is active in a number of areas including computational electromagnetics, electromagnetic bandgap structures and microwave metamaterials, antennas and radio propagation for body centric wireless networks, active antennas for millimeter/submillimeter applications and photonic integrated antennas. He is a co-editor and coauthor of the books *Antennas and Radio Propagation for Body-Centric Wireless Communications* (Boston, MA: Artech House, 2006), and *FDTD modelling of Metamaterials: Theory and Applications* (Boston, MA: Artech House, 2008), respectively.

Professor Hao is an Associate Editor for the *IEEE Antennas and Wireless Propagation Letters*, and was a Co-Guest Editor for the IEEE TRANSACTIONS ON ANTENNAS AND PROPAGATION. He is a member of Technical Advisory Panel of IET Antennas and Propagation Professional Network. He was elected as a Fellow of the ERA Foundation in 2007. He has served as an invited (ISAP'07, LAPC'07, IWAT'08) and keynote speaker (ANTEM'05), a conference General Chair (LAPC'08, Metamaterials'09), a Session Chair and short course organizer at many international conferences.